Electrical conduction in $(Bi_{0.5}Na_{0.5})_{0.94}Ba_{0.06}TiO_3$-PVDF 0-3 composites by impedance spectroscopy

Ansu Kumar Roy, Amrita Singh, Karishma Kumari, Kamal Prasad, Ashutosh Prasad[*]

University Department of Physics, T.M. Bhagalpur University, Bhagalpur 812007, India

Abstract: *The present work describes the use of ac complex impedance and electric modulus spectroscopy techniques to obtain the electrical parameters like electrical conductivity and activation energy of $(Bi_{0.5}Na_{0.5})_{0.94}Ba_{0.06}TiO_3$ (BNBT06)-PVDF 0-3 composites with (a) 10, (b) 20 and (c) 30 vol. percentage of BNBT06 in the frequency range 100 Hz–5MHz over a temperature range of 35^oC-$150°C$. SEM micrographs showed almost homogeneous distribution of grains with less porosity for all the compositions and the EDAX patterns confirmed the presence of different constituent elements of the composite samples. Complex impedance spectroscopic analysis indicated the presence of non-Debye type dielectric relaxation in the composites. The bulk resistance showed the NTCR character of the composite materials and the presence of grain-boundary effect along with the bulk contribution, especially in the lower frequency and higher temperature regime, was indicated by the modulus spectroscopic analyses, thus confirming the non-Debye type of multiple relaxations in the system. The ac electrical conductivity data as a function of temperature also endorsed the NTCR character of BNBT06-PVDF 0-3 composites. The ac conductivity based activation energy data allowed insight into the mechanism of the occurring conduction processes in the composite system which are explained on the basis of hopping model of charge carriers.*

Keywords- *Ceramic-polymer 0-3 composites; Grains /grain-boundaries; Hopping conduction; Complex impedance/ modulus spectroscopy; Ac conductivity; Activation energy*

I. INTRODUCTION

Ceramic-polymer composites form a new class of construction and functional materials of great potential applications in having combined hardness and stiffness of ceramics along with flexibility, elasticity, low density, and high breakdown strength of polymers and hence are being increasingly harnessed for their specific dielectric, ferroelectric, piezoelectric, pyroelectric, electro-optic, as well as superconducting properties in micro-devices [1]. During the last few years, increased global environmental concern has prompted considerable efforts to reduce the quantity of hazardous substances like the highly toxic lead in consumer products. Despite all these efforts, so far there has been no suitably harnessed material to replace ceramics such as the ubiquitous $(Pb, Zr)TiO_3$ (PZT), containing toxic lead, in various sensor/transducer applications. Piezoelectric ceramics have, in general, large dielectric constant, high piezoelectric charge coefficient as well as acoustic impedance, whereas polymers have generally lower dielectric constant and acoustic impedance close to that of water as well as of human body tissue. This low value of acoustic impedance combined with higher values of piezoelectric voltage coefficients for piezoelectric polymers makes them suitable candidates for mixing with piezoelectric ceramics in order to make good strain-monitoring and hydrostatic sonar sensors [2]. Further, these ceramic-polymer composite materials have been suggested to be viable alternative tools in piezoelectric and pyroelectric transducer applications [3]. Hence, piezoelectric composites are now an established alternative to conventional ferroelectric ceramic materials as well as to the more recently discovered ferroelectric polymers. In short, in view of the fact that these composites having excellent dielectric and mechanical properties can be prepared under lower temperature conditions and can be designed according to specific requirements by tailoring the relative fraction of the filler materials, these systems form the current area of active research activities and have received intensive global attention [4-6]. Recently, there has been a great interest in a new generation of composite materials exhibiting high dielectric performance with lower cost, size, weight, and easy processability due to widespread applications for the development of functional materials to fulfil the requirements of cheap, reliable, durable and environment-friendly batteries which are necessary for the most efficient energy storage and conversion device applications [7-11]. Towards a step forward in providing a lead-free perovskite ceramic material having optimal dielectric and piezoelectric properties, Takenaka [12], Wang *et al* [13], Lam *et al* [14], as well as the present group of workers [15] reported that the composition $(Na_{1/2}Bi_{1/2})_{0.94}Ba_{0.06}TiO_3$, which is near the morphotropic phase boundary(MPB) composition, is one of the most suited materials. As far as the polymer phase of the bi-phasic composite(s) is concerned, piezoelectric polymer PVDF, despite many of its lacking properties, has appeared appealing to numerous industries for its

inexpensive, lightweight, biologically compatible and mechanically stable structure. It can undertake large amount of deformation while sustaining large forces. It has expeditious response time, very low density, and distinguished flexibility when compared to those of electro-active ceramics and shape memory alloys. The piezoelectric PVDF and its copolymers are widely used materials in both actuation and sensing appliances. The AC electrical studies of the polymers reveal some structural details and add valuable complementary information relevant to electrical applications of ceramic-polymer composite materials. The contribution of polymer to grain (bulk), grain boundaries and the electrode effects can be studied by frequency dependent measurements and thus it can give the valuable information related to microstructural details about electrical applications of polymer materials [16]. Further, it is well known that the complex impedance spectroscopy (CIS) is a powerful tool for characterizing the dynamics of bound or mobile charges in the bulk or interfacial regions of any kind of solid or liquid material: ionic, semiconducting, mixed electronic– ionic, and even insulators (dielectrics) and complex modulus spectroscopy (CMS) is an alternative approach to explore electrical properties of the material and magnify any other effects (which are unidentifiable or superimposed on the others in the CIS technique) present in the sample. It is an important and convenient tool to determine, analyze and interpret the dynamical aspects of electrical transport phenomena (i.e. parameters such as carrier/ion hopping rate, conductivity relaxation time, etc.). In the heterogeneous system (i.e., mixed state of polymer + ceramic), it is necessary to explain the impedance spectroscopy along with the modulus spectroscopy to understand the complete relaxation and conduction mechanism present in the samples. In the polymer phase, segmental chains are involved in the relaxation process [17] whereas in ceramic phase, dipoles are involved and the conductivity of two systems is different in nature. An extensive literature survey revealed that the ac conductivity studies on $(Bi_{0.5}Na_{0.5})_{0.94}Ba_{0.06}TiO_3$ (BNBT06)-PVDF (ceramic-polymer) 0-3 composites in the light of complex impedance and electric modulus spectroscopy have not been undertaken in the recent past. In view of the aforesaid facts, the present work relating to the study of the ac conduction in BNBT06/PVDF 0-3 composite samples having 10, 20 and 30 volume percent of BNBT06 powder via complex impedance and electric modulus spectroscopy analyses has been undertaken.

II. EXPERIMENTAL PROCEDURE

Polycrystalline ceramic samples of $(Bi_{0.5}Na_{0.5})_{0.94}Ba_{0.06}TiO_3$ were prepared by a high-temperature solid-state reaction technique at 1160ºC for about 3h and the fabricated compact green pellets were sintered at an optimized temperature of 1180ºC for about 2h.in air atmosphere. The XRD patterns at the room temperature were observed on calcined powder of BNBT06 with an X-ray diffractometer (X'pert-PRO, USA), using Cu K_α radiation (λ=1.5405 Å) over a broad range of Bragg angles (20º≤2θ≤80º). The patterns confirmed the tetragonal unit cell structure for the ceramic. BNBT06/PVDF 0-3 composite samples having 10, 20 and 30 volume percentage of BNBT06 powder were fabricated by solution cast method (using DMF as the solvent for PVDF) at an elevated temperature (~70ºC-80ºC) under constant stirring with the help of a magnetic stirrer. The composite samples in the molten (viscous) state were poured into shallow cylindrical and rectangular stainless steel dies and then were allowed to dry for a few days in open air. The fabricated composites were taken out of the dies and were then cut into the disk-shaped pieces of suitable thicknesses and were allowed to dry further before any measurements on them were made. The green samples were then polished and painted on both sides by the use of high grade silver paste (Ted Pele, USA). Microstructures of the fabricated composites were observed at room temperature by using a scanning electron microscope (JEOL-JSM840A).The room temperature dielectric constant (ε_r) and loss tangent (tanδ) (and hence dielectric loss as well as the ac conductivity) of the different composite samples were evaluated in the frequency range 100Hz-5 MHz and between the ambient temperature and 150ºC through the use of capacitance (C_p) data provided by a computer interfaced LCR Hi-Tester (HIOKI 3532-50, Japan) on a symmetrical cell of type Ag| *Composite*| Ag, where Ag is a conductive paint coated on either side of the pellet.

III. RESULTS AND DISCUSSION

Figure 1 shows the EDAX patterns and SEM micrographs (insets) for the BNBT06-PVDF 0-3 composites having (a) 10, (b) 20 and (c) 30 vol. % of BNBT06 ceramic fillers. SEM micrographs of the fractured surfaces showed that the particle distribution in the grains is not strictly homogeneous. Some areas of agglomeration of particles in the grains are also seen in the micrographs. EDAX patterns confirmed the presence of different constituent elements of the composite samples like Bi, Na, Ba, Ti, O, C etc.
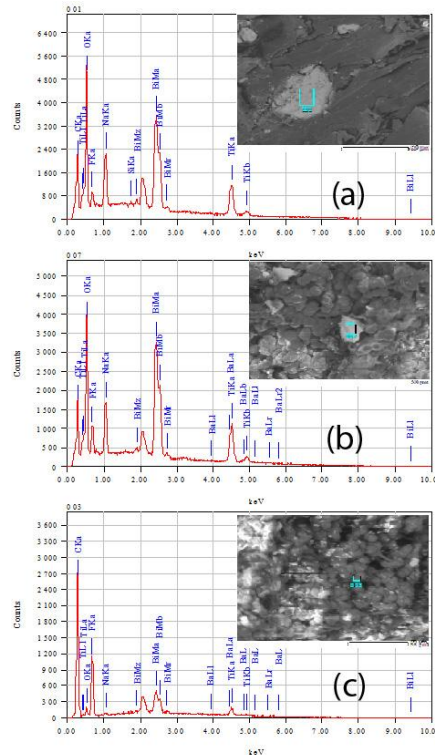
Fig. 1 EDAX patterns and SEM micrographs (insets) of (Bi$_{0.5}$Na$_{0.5}$)$_{0.94}$Ba$_{0.06}$TiO$_3$(BNBT06)-PVDF 0-3 composites having (a) 10, (b) 20 and (c) 30 vol.% of BNBT06.

Figure 2 (a)-(c).shows the Z$'$ (*f*) and Z$''$ (*f*) plots for BNBT06-PVDF 0-3 composites having (a) 10, (b) 20 and (c) 30 vol. % of BNBT06 ceramic fillers at several temperatures between ambient temperature and 150°C. From the plots it is seen that at lower temperatures Z' is found to decrease monotonically with increasing frequency up to a certain limiting frequency (~10kHz) above which it becomes almost frequency independent. The higher values of Z$'$ at lower frequencies and higher temperatures means the polarization in the test material is larger. The temperature where this frequency-dependent to frequency-independent change of Z' occurs, varies with frequency in different material compositions. This also signifies that the resistive grain boundaries become conducting at these temperatures and that the grain boundaries are not relaxing even at the highest measurement ranges of frequency and temperature. Z$''$(*f*) plots showed almost identical monotonically decreasing type of variation up to a certain frequency limit ~10kHz beyond which they merge together at a very low value of Z$''$ to show frequency- independent nature of variation extending up to the highest frequency limit at all the chosen temperatures. The merger of Z$''$ (as well as of Z$'$) at higher frequencies for all the temperatures indicate possible release of space charge polarization/accumulation at the boundaries of homogeneous phases in the test material system under the applied external field. At lower temperatures, monotonic decrease of Z$''$ indicated that at lower temperatures the relaxation is absent in the material system. This means that relaxation species are immobile defects and the orientation effects may be associated. Also, the decreasing magnitudes of Z$'$ and Z$''$ with increasing frequencies would imply that relaxation in the material system is temperature-dependent, and there is apparently not a single relaxation time. Fig (d) (from top to bottom) shows the frequency dependent variation of real and imaginary parts (Z$'$ and Z$''$), respectively, for the three compositions at the room temperature. From the plots it is seen that in the lower frequency region the magnitude of Z$''$ decreases from ~110 MΩ to 60 MΩ with increase in volume content of the ceramic filler from 10% to 30%, as shown in the *bottom figure*. However, the trend of ceramic filler concentration dependent variation of Z' in the lower frequency region is just opposite to that of Z$''$ in the sense that it increases from ~9.5 MΩ to 12 MΩ with an increase in volume content of the ceramic filler from 10% to 30%, as shown in the upper half of Fig. 2(d), thereby showing an increased resistive grain boundaries' contribution with increase in volume content of the ceramic filler in the composite.
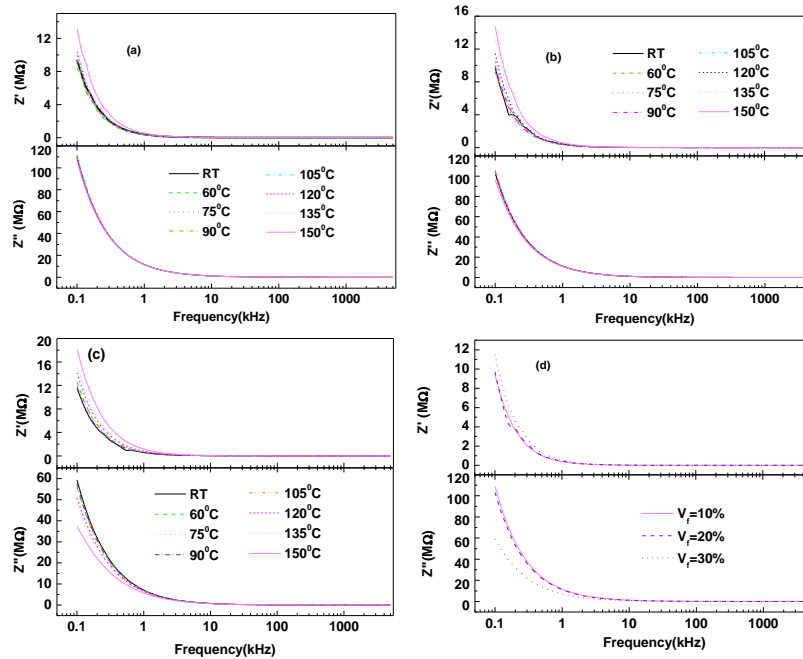
Fig. 2(a)-(c) Frequency dependent variation of real and imaginary parts (Z' and Z'') of complex impedance (Z*) of (Bi$_{0.5}$Na$_{0.5}$)$_{0.94}$Ba$_{0.06}$TiO$_3$ (BNBT06)-PVDF 0-3 composites having (a) 10, (b) 20 and (c) 30 vol. percentage of BNBT06 at different indicated temperatures. Fig.(d) (from up to down) shows the frequency dependent variation of real and imaginary parts (Z' and Z''), respectively, for the three compositions at the room temperature

Complex Impedance spectroscopy (CIS) is a powerful tool for characterizing many of the electrical properties of materials and their interfaces with electronically conducting electrodes. It may be used to investigate the dynamics of bound or mobile charges in the bulk or interfacial regions of any kind of solid or liquid material: ionic, semiconducting, mixed electronic–ionic, and even insulators (dielectrics). The CIS gives the direct correlation between the response of a real system and an idealized model circuit composed of discrete electrical components. An equivalent circuit based on impedance and electric modulus spectra provides the physical explanation to the processes occurring inside the material system. Most of the real ceramics contain grains and grain-boundary regions, which individually have very different physical properties. These regions are well observed in the impedance and modulus spectra. Electrical *ac* data may be presented in any of the four interrelated formalism: Relative permittivity (ε^*) = ε'- jε''; Impedance (Z^*) = Z'+ jZ'' = $1/j\omega C_0\varepsilon^*$; Electric modulus ($M^*$) = $M' + jM'' = 1/\varepsilon^*$; Admittance ($Y^*$) = $Y' + jY'' = j\omega C_0\varepsilon^*$; and tan $\delta = \varepsilon''/\varepsilon' = M'' /M' = Z'/Z'' = Y''/Y'$, where $\omega(=2\pi f)$ is the angular frequency; C_0 (= $\varepsilon_0 A/t$) is the geometrical capacitance; j = $\sqrt{-1}$; ε_0 is the permittivity of free space (=8.854$\times10^{-12}$ Fm^{-1}); *t* and *A* are the thickness and area of the pellet; and δ is complementary to the phase angle (θ), as observed by the LCR Hi-Tester.

The electrical properties of the present composite material system have been first investigated using Complex Impedance Spectroscopy (CIS) technique. The Nyquist plots between Z' (*f*) and Z''(*f*) (actually, it is -Z'', but for the sake of convenience only the modulus of the quantity (Z'') has been used in all of the plots drawn in the present work) for BNBT06-PVDF 0-3 composites having (a) 10, (b) 20 and (c) 30 vol. % of BNBT06 ceramic fillers at several temperatures between ambient temperature and 150°C are observed. The impedance spectrum is distinguished by semicircles. A series array of lone parallel RC combination (R_g, C_g) in series with a resistor (R_s) (though the almost frequency-independent data of R$_s$ are not shown in any of the plots, for brevity sake) was found to best fit the experimental data for the given composition, thereby indicating the contribution from intrinsic grains in the samples. No other relaxation mechanism, such as the grain-boundaries or electrode effects in the sample could be identified through the CIS technique in the studied frequency range. A single semicircle indicates that only one primary mechanism is responsible for the electrical conduction within the sample between the temperature of ambience and 150°C.In other words, the absence of other semicircles in the complex impedance plots suggest the dominance of bulk contributions in the composite. With increasing temperature, intercept points on the real axis are shown to shift towards the origin. However, the different semicircles from whose radii R$_g$ were evaluated for the composite having 30 vol. % of the ceramic filler corresponding to the different measurement temperatures have not been shown in the plots, for brevity sake.
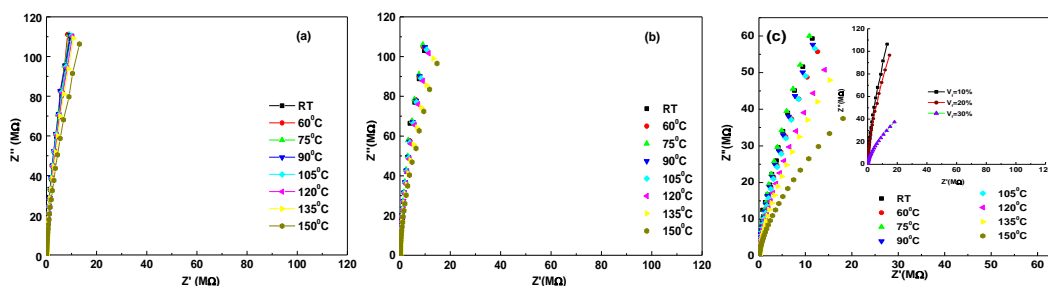
Fig. 3(a)-(c) Complex impedance plots for (Bi$_{0.5}$Na$_{0.5}$)$_{0.94}$Ba$_{0.06}$TiO$_3$ (BNBT06)-PVDF 0-3 composites having (a) 10, (b) 20 and (c) 30 vol. percentage of BNBT06 at different indicated temperatures. Insert to Fig. (c) shows the complex impedance plots for the three compositions at the room temperature.
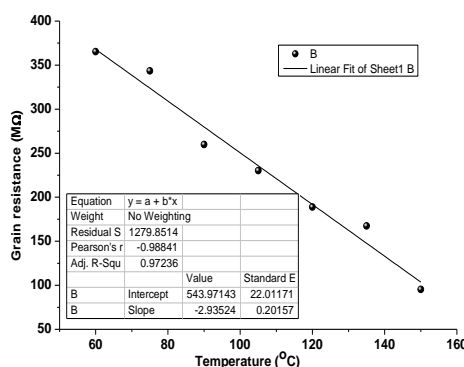
Fig. 4 Variation of grain resistance vs. temperature for (Bi$_{0.5}$Na$_{0.5}$)$_{0.94}$Ba$_{0.06}$TiO$_3$ (BNBT06)-PVDF 0-3 composites with 30 vol. percentage of BNBT06. Insert to the figure shows the linear fitting parameters for the variation.

Figure 3(a)-(c) shows temperature-dependent impedance spectra (Nyquist plots) of (Bi$_{0.5}$Na$_{0.5}$)$_{0.94}$Ba$_{0.06}$TiO$_3$ (BNBT06)-PVDF 0-3 composites having (a) 10, (b) 20 and (c) 30 vol. percentage of BNBT06. It was observed that for the composites having 10 and 20 volume percentage of the ceramic filler showed very high order of insulating properties in giving plots in the form of almost straight lines parallel to the ordinate, as is evident in Fig. 3(a) and 3(b). However, the resulting curves for the composite having 30 volume percentage of the ceramic filler, as shown in Fig.3(c), showed a tendency to bend towards the abscissa to form semicircles with their centres below the real axis, having comparatively larger radii and the radii decreasing with the increase of temperature, thereby representing the distribution of relaxation times in the test sample and indicating a decrease in the resistivity of the material with a clear-cut departure from the ideal Debye type behaviour. Figure 4 shows the temperature dependence of bulk resistance of BNBT06-PVDF 0-3 composite having 30 vol. percentage of BNBT06 evaluated from the semicircles of the Nyquist plots shown in Fig. 3(c). It indicates that the grain resistance monotonically decreases with increasing temperature and it shows the maximum and minimum values of about 370 MΩ and 100 MΩ at 60°C and 150°C, respectively. A reasonably good linear fit (r^2 ~0.97) to this variation is also shown along with the plot with the fitting parameters inserted.

Complex modulus analysis is an alternative approach to explore electrical properties of the material and magnify any other effects present in the sample (which are unidentifiable or superimposed on the others in CIS technique) as a result of different relaxation time constants. It is an important and convenient tool to determine, analyze and interpret the dynamical aspects of electrical transport phenomena (i.e. parameters such as carrier/ion hopping rate, conductivity relaxation time, etc.). In order to analyze and interpret the experimental data, it is essential to have a model equivalent circuit that provides a realistic representation of the electrical properties. The modulus representation suppresses the unwanted effects of extrinsic relaxation often used in the analysis of dynamic conductivities of ionically conducting glasses. The dielectric modulus (M*=1/ ε*) is frequently used in the analysis of dielectric data of ionic conductors [18]. The advantage of adopting complex electrical modulus spectra is that it can discriminate against electrode polarization and grain boundary conduction process. Using electric modulus analysis, it is easier to relate this phenomenon to other properties, especially the dynamical mechanical modulus and can be written as a single function of conductivity. Sinclair and West [19, 20] suggested the combined usage of impedance and modulus spectroscopic plots to rationalize the dielectric properties. Only one peak in Z"(*f*) vs. Z' (*f*) plots but two peaks in M" (*f*) vs. M' (*f*) plots at all the test temperatures for all the compositions taken for analysis in the present study suggest that the impedance data can be better analyzed by re-plotting them in the modulus formalism. The peak heights are proportional to *R* for

the Z$''$(*f*) vs. Z$'$ (*f*) plots and to C^{-1} for the M''(*f*) vs. M'(*f*) plots. Complex impedance plane plots of Z'' versus Z' (where Z' and Z'' are the real and imaginary parts of the complex impedance (Z*), respectively) are useful in determining the dominant resistance of a sample but are insensitive to the smaller values of resistances. Similarly, complex modulus plots are useful in determining the smallest capacitance. Thus, the power of combined usage of both impedance and modulus spectroscopy is that the Z'-Z'' plot highlights the phenomenon of largest resistance whereas *M''* vs. M' picks up those of the smallest capacitance [21]. The additional contribution in the low frequency part to the specific semicircle is attributed to the blocking effect of the pores. Also, the poor separation of the overlapped semicircles is ascribed to the blocker (pore) size and if the blocker size is greater than 1μm, it would lead to the overlapping of the semicircles [22].

Figure 5(a) and 5(b) shows the complex modulus plane plots for these compositions (having 10 and 20 vol. percentages of BNBT06) corresponding to the highest temperature of measurement i.e., at 150°C. Both the plots provide almost touching semicircles for grains and grain-boundaries with dominant grain-boundaries whereas the grain-boundaries could not be identified in the complex impedance plane (Nyquist) plots for the same compositions at the given temperature. These semicircles indicate that both grain and grain boundary capacitance started playing active roles in the conduction mechanism of the material system at higher temperatures.
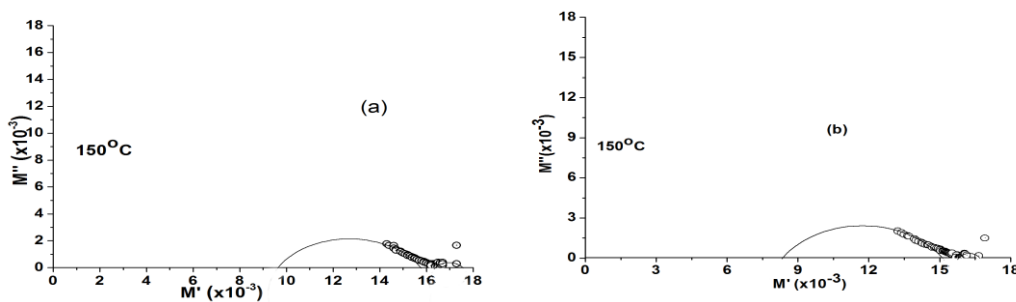

Fig. 5(a) & (b) Complex modulus plots corresponding to 150°C for (Bi$_{0.5}$Na$_{0.5}$)$_{0.94}$Ba$_{0.06}$TiO$_3$ (BNBT06)-PVDF 0-3 composites with (a) 10, (b) 20 vol. percentages of BNBT06.
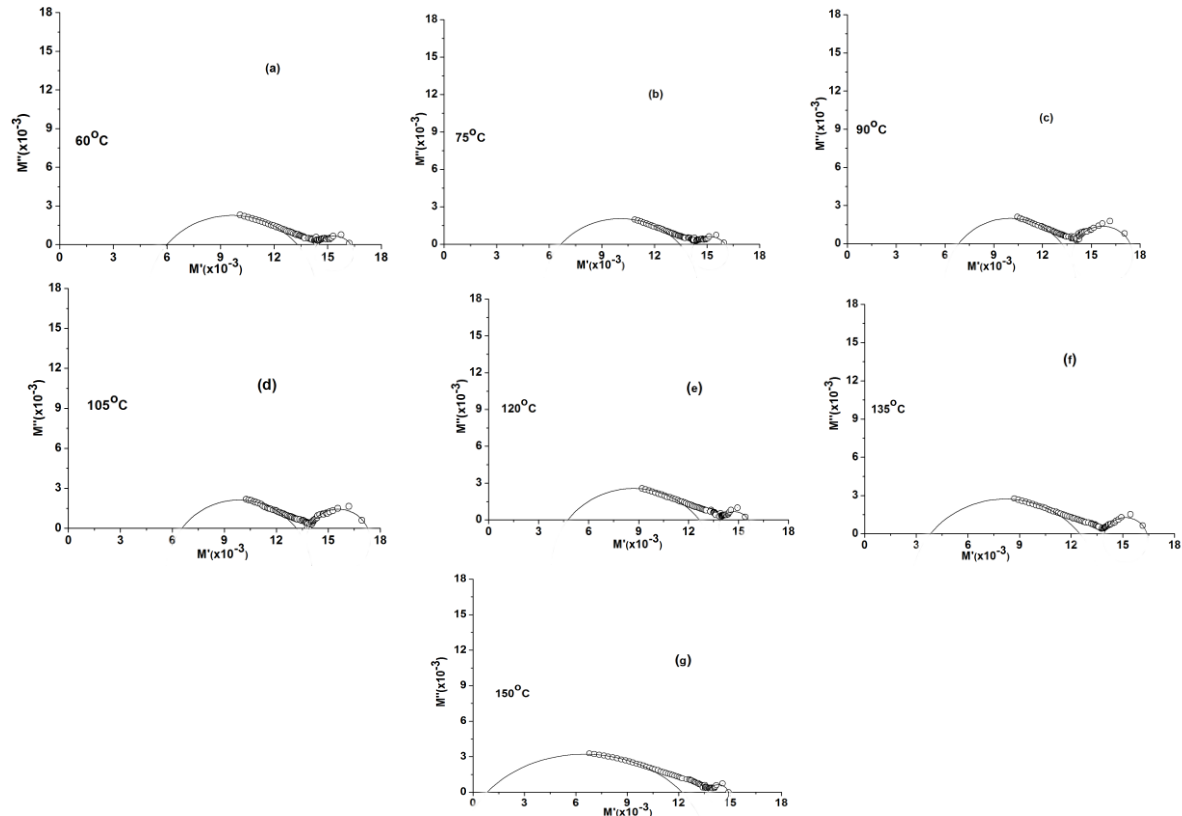

Fig. 6(a)-(g) Complex modulus plots for (Bi$_{0.5}$Na$_{0.5}$)$_{0.94}$Ba$_{0.06}$TiO$_3$ (BNBT06)-PVDF 0-3 composites having 30 vol. percentage of BNBT06 corresponding to (a) 60°C, (b) 75°C, (c) 90°C, (d) 105°C, (e) 120°C, (f) 135°C, and (g) 150°C.

Figure 6(a)-(g) shows the complex plane plots (M'' vs. M' plots) for BNBT06-PVDF 0-3 composite having 30 vol. % of BNBT06 drawn at different temperatures between 60°C-150°C at an equal interval of 15°C. All these plots indicate the contribution of grain-boundaries along with grains in the process of charge transport inside the test composite. It is further seen that at lower temperatures the two semicircles corresponding to the grains and grain-boundaries appear almost touching each other with the dominant grain-boundaries (in view of larger semicircle for the grain-boundaries than that due to grains in all the cases) which act as barriers to the cross transport of charged carriers. Furthermore, with increasing temperatures the two semicircles gradually appear to separate from each other. At the same time, the radii of the grain-boundary semicircles go on increasing with increasing temperature, thereby showing the increasing dominance of the grain-boundary effect with the increase in temperature for PVDF-BNBT06 0-3 composite having 30 vol. % of BNBT06. As shown in Fig. 6(g), the two semicircles appear clearly separated from each other with the largest semicircle for the grain-boundaries and smallest one for the corresponding grains, thereby showing the maximum dominance of grain-boundaries over the grains in the given composition at the highest measurement temperature. Though the value of M'' corresponding to the peaks is very low, but it is also seen to depend on the ceramic filler content in the composites. At the highest measurement temperature i.e. at 150°C, M'' at the peak exhibits slight decrease (and the corresponding increase in capacitance C) as we see the two compositions having 10 vol. percent to 20 vol. percent of the ceramic filler, as shown in Fig. 5(a) and 5(b), respectively. On the other hand, an increase in peak M'' (indicating a decrease in capacitance C) is shown for the composite having 30 vol. percent, as shown in Fig. 6(g). The imaginary parts of impedance and electric modulus are expressed as:

$$Z'' = R[\omega RC / \{1 + (\omega RC)^2\}] \hspace{3cm} 1(a)$$

$$M'' = (C_0 / C)[\omega RC / \{1 + (\omega RC)^2\}] \hspace{2cm} 1(b)$$

given by:

$$\omega_{max} = 1/RC = \tau^{-1} \hspace{4cm} (2)$$

From the above equations (1) and (2) the peak values of the imaginary parts of impedance and electric modulus are given as:

$$Z''_{max} = R/2 \hspace{5cm} 3(a)$$

and

$$M''_{max} = C_o / 2C \hspace{4.5cm} 3(b),$$

where C_0 (= ε_0A/t) is the geometrical capacitance; ε_0 is the permittivity of free space, 8.854×10^{-12} Fm^{-1}; t and A are the thickness and area of the pellet, as referred to earlier. Using the M''_{max} values from the semicircles corresponding to the grains of the samples in the $M'' = f(M')$ plots for BNBT06-PVDF 0-3 composite having 30 vol. percentage of BNBT06 drawn at 120°C, 135°C and 150°C, as shown in Fig. 6(e)-(g), and the samples' specifications like t and A along with the permittivity of free space (ε_0), C-values corresponding to the modeled *RC* circuit for the grains of the test sample were found out at those three temperatures. The spectra corresponding to 120°C, and 150°C, as shown in Fig. 6(e) and 6(g), respectively, indicated an increase in grain capacitance from 0.184 nF to 0.214 nF and hence a decrease in the grain resistance of the sample with increase in temperature [23]. It endorsed the NTCR type behaviour of the material. However, the peak corresponding to 135°C showed an increase in peak height of the right semicircle and consequent decreased value (~0.115 nF) in grain capacitance as compared with that corresponding to 120°C and 150°C. A similar increase in frequency exponents i.e., the low and high frequency hopping parameters (s_1 and s_2) at 135°C has been observed (as may be seen later in Fig. 9).These results show a type of transition temperature at 135°C for the dominant hopping conduction taking place inside the test material.. In the light of the above, peak heights of the left semicircles in Fig. 6(e), 6(f), and 6(g) corresponding to the grain-boundaries were also analyzed. From the plots it is seen that on increasing the temperature from to 120°C 150°C, the peak heights of the semicircles corresponding to the grain-boundaries increase from about 0.0026 to 0.0032, thereby indicating a decrease in grain-boundary capacitance and corresponding increase in grain-boundary resistance of the sample (since grain-boundary capacitance, C$_{gb}$, is inversely proportional to its resistance, R$_{gb}$) with increase in temperature. It indicates the positive temperature coefficient of resistance (PTCR) type behaviour of the grain-boundaries of the test material. These results support the views of Sinclair and West [19, 20] that the inner fraction of a grain has semiconducting properties, whereas the grain-boundaries have insulating properties.

The real part of ac conductivity is given by:

$$\sigma'_{ac} = \omega \varepsilon_o \varepsilon'' = \omega \varepsilon_0 \varepsilon_r \tan \delta \hspace{3cm} (4)$$

where $\omega = 2\pi f$, (*f* being the frequency used); ε_o is the permittivity of free space (= 8.854 x 10^{-12} Fm^{-1}) and ε'' is the dielectric loss factor, as referred to earlier. Thus, σ'_{ac} is directly related to the dielectric properties of the material. Alternatively, the real part of the dominant bulk conductivity may be evaluated from the impedance

spectrum using the relation $\sigma'_{ac} = t / (Z'A)$; where Z' is the real part of complex impedance (intersection of semicircle on the real-axis in Z'' vs. Z' plot); t the thickness, and A the surface area of the sample.
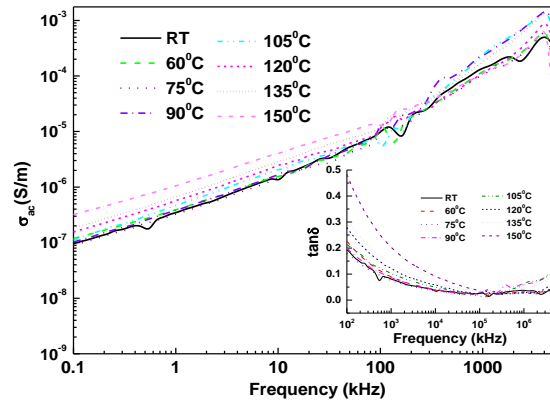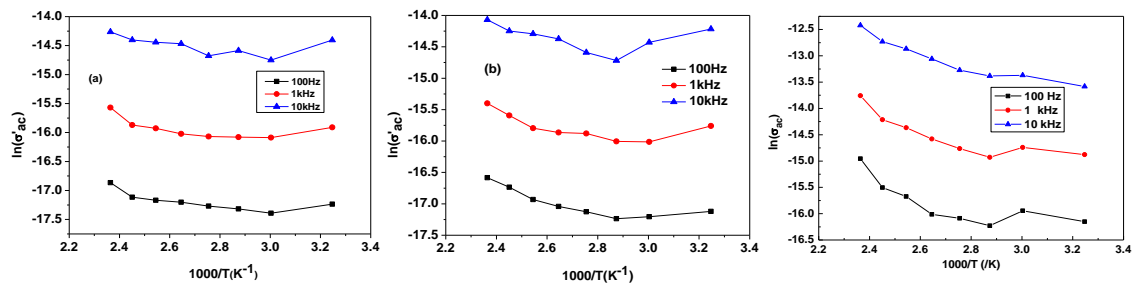

Fig. 7. Frequency dependence of real part of AC conductivity for (Bi$_{0.5}$Na$_{0.5}$)$_{0.94}$Ba$_{0.06}$TiO$_3$ (BNBT06)-PVDF 0-3 composites with 30 vol. percentage of BNBT06 at different indicated temperatures. Inset: Frequency dependent loss factor of the composite at different temperatures.

Figure 7 shows the log-log plot of the real part of ac electrical conductivity (σ'_{ac}) versus frequency at different temperatures for BNBT06-PVDF 0-3 composite having 30 vol. % of BNBT06 filler. From the plot it is observed that the real part of ac conductivity changes by about three to four orders of magnitude in the measurement ranges of frequency (from 100 Hz to 5 MHz) and temperature (from the temperature of ambience to 150°C).The plot indicated that the present material exhibited a low frequency dielectric dispersion (LFDD). Further, all the σ'(f) curves were found to be merging at a high frequency (at ~500kHz) above which an opposite dispersion was observed, thereby suggesting the less defect mobility and low conductivity in the material [20].Furthermore, all the σ'(f) curves (as shown in Fig.7) corresponding to the different measurement temperatures are shown to provide sharp peaks in ac conductivity values at about 4 MHz beyond which the conductivity showed a sharp fall, with the sharpest fall at the highest measurement temperature i.e., at 150°C. This type of variation in ac conductivity in the highest measurement frequency region is due to the sudden enhancement in dielectric loss factor, as is evident in the inset of Fig. 7. Each of the curves clearly indicated at least two slopes-one in the lower and the other in the higher frequency region. The frequency dependence of ac conductivity does not seem to follow the simple Jonscher's power law. On the other hand, it is seen to follow a double power law [23-28] given as:

$$\sigma_{ac} = \sigma_o + A\omega^{S_1} + B\omega^{S_2} \tag{5}$$

where σ_o is the frequency independent (electronic or dc) part of ac conductivity. The exponent s_1 ($0 \leq s_1 \leq 1$) characterizes the low frequency region i.e., to the grain-boundary conductivity, corresponding to translational ion hopping whereas the exponent s_2 ($0 < s_2 < 2$) characterizes the high frequency region i.e., to the grain conductivity indicating the existence of well localized relaxation/re-orientational process [26], the activation energy of which is ascribed to the reorientation ionic hopping. In the jump relaxation model (JRM) introduced by Funke [27] and extended by Elliot [28] to account for ionic conduction in solids, there is a high probability for a jumping ion to jump back (unsuccessful hop). However, if the neighbourhood becomes relaxed with respect to the ion's position, the ion stays in the new site. The conductivity in the low frequency region is associated with successful hops. Beyond the low frequency region, many hops are unsuccessful and as the frequency increases, there is higher possibility of more hops to be unsuccessful. The change in the ratio of successful to unsuccessful hops results in dispersive conductivity in the test material(s). In the perovskite type oxide materials, presence of charge traps in the band gap of the insulator is expected. The JRM suggests that different activation energies are associated with unsuccessful and successful hopping processes. The frequency and temperature dependence of ac conductivity in the BNBT06-PVDF 0-3 composites resembles that of hopping type conduction. Applying JRM to the frequency response of the conductivity for the test materials, experimental conductivity data were found to fit the double power law as given in Equation (5).

Fig. 8. (a)-(c) Variation of log of the real part of ac conductivity with inverse absolute temperature for $(Bi_{0.5}Na_{0.5})_{0.94}Ba_{0.06}TiO_3$ (BNBT06)-PVDF 0-3 composites having (a) 10, (b) 20 and (c) 30 vol. percentages of BNBT06 at different indicated frequencies.

Figure 8(a)-(c) shows the $\ln(\sigma'_{ac})$ *vs.* $1000/T$ plots for the three compositions i.e.,10, 20, and 30 volume percentage of BNBT06 at 100 Hz,1kHz, and 10kHz. It is observed from these plots that in the low temperature regime, ac conductivity of all the compositions increased with increase in frequency, however a bit slowly, thereby indicating dispersion of conductivity with frequency. With increase in temperature, dispersion in conductivity narrowed down and all the curves for different frequencies appeared to merge at high temperatures, although they didn't merge completely. The activation energy for conduction was obtained using the Arrhenius relationship:

$$\sigma_{ac} = \sigma_o \exp(-E_a / k_B T) \qquad\qquad 6(a)$$

whence $\ln(\sigma'_{ac}) = \ln(\sigma_o) - E_a/k_B T$ $\qquad\qquad 6(b)$

The slope of the linear least-squares-fit of the conductivity data to Eq. 6(b) gives the value of the apparent activation energy, E_a. The ac activation energies were calculated in two different temperature regions at different frequencies using the Arrhenius relation (Eq. 6) and the values are given in the Table 1. It is observed that ac conductivity-based activation energy calculated at higher frequencies is lower than that at lower ones in the same temperature range for all the compositions, especially for the composite having 30 volume % of the ceramic filler. The conductivity-based activation energies for BNBT06-PVDF 0-3 composites having 10 and 20 vol. percentages of BNBT06 are found to be in the limiting range of 0.042-0.138 eV and 0.055-0.177 eV in the lowest and highest ranges of frequency measurement, respectively, as reported in Table 1. Further, the ac conductivities for these compositions have comparatively larger values at higher temperatures than those at lower ones. It is due to the fact that when the temperature is increased, the mobility of polymer chain is enhanced and the fraction of free volume in the polymer composite increases. Accordingly, oxygen vacancies get enhanced in the modified ceramics. Hence, the fraction of free volume in the polymer composite facilitates the translational motion of charge carriers and hence higher values of activation energies of the conduction process in the higher temperature range for all the composite samples. However, the conductivity based activation energies for the other two compositions (having. 10 and 20 volume % of the ceramic filler) do not seem to be very reliable and useful for analysis based on them in the sense that these composites have exhibited very high order of magnitudes of resistivity, as indicated in Fig. 3(a) and 3(b). This is due to the fact that at low frequencies the overall conductivity is due to the mobility/transportation of charge carriers over long distance rather than from relaxation/ orientational mechanism in which case the charge mobility/transportation is restricted to only the nearest neighbouring lattice sites. The merger of the conductivity curves in the higher temperature region results with the release of space charge, thereby endorsing the results derived from the Complex Impedance Spectroscopic analyses. In the low temperature region (60 °C -120°C), the activation energies for BNBT06-PVDF 0-3 composites with (a) 10, (b) 20 and (c) 30 vol. percent of BNBT06 measured at 1 kHz are in the range of 0.028-0.146 eV. In this region, conductivity is almost independent of temperature and this low value of activation energy corresponds to the intrinsic conduction in the test material system. The activation energies ~0.298-0.452eV in the higher temperature region (135-150°C) thus showed a sharp increase with an increase in temperature, thereby suggesting that the conductivity may be the result of defects and associated charge carriers of metal ions such as Na^+, Bi^{3+}, and Ba^{2+} in the ceramic phase of the composite. At higher sintering temperatures, bismuth ions are the first to get evaporated and thereby oxygen vacancies are created for charge neutralization. Defects such as bismuth $V_{Bi}^{\bullet\bullet\bullet}$ and oxygen vacancies $V_O^{\bullet\bullet}$ are considered to be the most mobile charges and play an important role in polarization fatigue and conduction [25]. The enhancement in conductivity with temperature may be considered on the basis that within the bulk, the oxygen vacancies due to the loss of oxygen (usually created during sintering) allow the charge compensation process

following the Kröger-Vink equation [25]: $O_o \rightarrow \frac{1}{2}O_2 \uparrow + V_o^{\bullet\bullet} + 2e^{-1}$ to occur, thereby showing that free electrons are left behind in the process, making the materials n-type.

TABLE 1. AC Conductivity based activation energy for $(Bi_{0.5}Na_{0.5})_{0.94}Ba_{0.06}TiO_3$ (BNBT06)-PVDF 0-3 composites having 10, 20 and 30 vol. percentages of BNBT06 at different indicated frequencies in the low and high temperature ranges.

Volume fraction (%) of the filler	Conductivity based activation energy (eV)					
	100 Hz		1 kHz		10 kHz	
	60 °C-120°C	135 °C-150°C	60 °C-120°C	135 °C-150°C	60 °C-120°C	135 °C-150°C
10	0.042	0.248	0.028	0.298	0.055	0.138
20	0.055	0.149	0.043	0.191	0.117	0.177
30	0.135	0.543	0.146	0.452	0.138	0.306
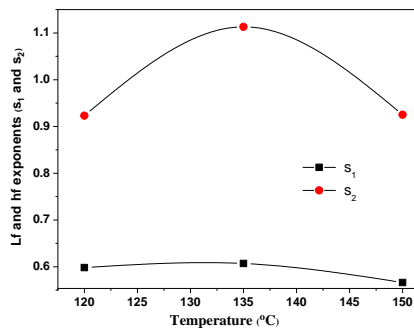
Fig. 9 Temperature dependence of low and high frequency hopping parameters (s_1 and s_2) for $(Bi_{0.5}Na_{0.5})_{0.94}Ba_{0.06}TiO_3$ (BNBT06)-PVDF 0-3 composites with 30 vol. percentage of BNBT06, between in the temperature range of 120°C-150°C.

Figure 9 shows the temperature–dependent variations of the exponents, (s_1 and s_2) for BNBT06-PVDF 0-3 composite having 30 vol. percent of BNBT06 filler between 120-150°C. In the present work, s_1 represents the exponent evaluated between the frequency limits of 100Hz to 54kHz and s_2 has been evaluated between 64kHz and 1 MHz. From the plots it is manifested that s_1 assumes a maximum value ~0.607 at 135°C and s_2 assumes a maximum value ~1.113 at the same temperature for the given composition. Due to localization of charge carriers, formation of polarons takes place and the hopping conduction may occur between the nearest neighbouring sites. The value of s_1 first increases with temperature up to 135°C and then decreases. The nature of conduction has a remarkable relationship with these slopes [28, 31]. For small polaron hopping conduction, the value of s increases with temperature, while for large polaron hopping conduction s decreases with temperature [32]. Here, the value of s_1 first increases because of the dominance of small polaron hopping mechanism [30]. After 135°C, the slope decreases because of large polaron hopping mechanism (because the mobility of large polarons is proportional to $T^{-1/2}$). Small polaron formation takes place in those materials whose conduction band belongs to the incomplete "*d*" or "*f*" orbital [30]. In the present case, Ti^{3+} may be assumed to be present in the test composite samples due to the reduction of Ti^{4+} of the BNBT06 ceramic constituent into Ti^{3+}, thereby creating incomplete "*d*" orbital which may possibly be responsible for the small polaron formation. These polaronic states may be thermally dissociated and the residual carriers can form a large polaron due to the interaction with the positive ions in the lattice. The small polaron hopping mechanism is a thermally activated one. Thus as temperature increases, conductivity increases and s_1 increases. But as the temperature exceeds 135°C, charge carriers trapped in the potential well can form large polarons. These large polarons are easily scattered by the ions and phonons in the material. Thus, the change in conductivity ($\Delta \sigma'_{ac}$) with increase in temperature decreases i.e., s_1 decreases with an increase in temperature. Since the trapped carrier of a large polaron extends over multiple sites, the carrier can continuously adjust to the alternations of the atomic positions and thereby move between sites coherently [33]. Hence, the conductivity increases with the increase in temperature. The value of s_2 has also a decreasing trend with increase in temperature beyond 135°C. A similar explanation to the temperature-dependent variations of s_2, as for s_1, also holds good. In the light of the resulting frequency- and temperature-dependent ac conductivity data for $(Bi_{0.5}Na_{0.5})_{0.94}Ba_{0.06}TiO_3$ (BNBT06)-PVDF 0-3 composites, it may be inferred that the JRM for the hopping of charge carriers seems to hold good in the entire frequency range for the test material system.

IV. CONCLUSION

The present work describes the mechanism of the conduction processes in (Bi$_{0.5}$Na$_{0.5}$)$_{0.94}$Ba$_{0.06}$TiO$_3$ (BNBT06)-PVDF 0-3 composites by the use of impedance and electric modulus spectroscopic techniques. X-ray diffraction data confirmed the formation of phase pure compounds in all the compositions. SEM micrographs showed that the particle distribution in the grains is not strictly homogeneous. Some areas of agglomeration of particles in the grains are also seen in the micrographs. EDAX patterns confirmed the presence of different constituent elements of the composite samples like Bi, Na, Ba, Ti, O, C, etc. Simultaneous use of complex impedance and electric modulus spectroscopic analyses in the composite samples in the frequency range 100 Hz–5 MHz over a wide temperature range 35°C-150°C indicated the presence of grain-boundary effect along with the bulk contribution, especially at higher temperatures, and also confirmed the presence of non-Debye type of multiple relaxations in the materials. Conduction mechanism in the material system is explained on the basis of Jump Relaxation hopping model of charge carriers. The electrical conductivity data as the function of temperature suggest the negative temperature coefficient of resistance behaviour of the test ceramic-polymer composites. The ac conductivity based activation energies for the test composite material system have also been estimated.

Acknowledgement

REFERENCES

[1] M. Goel, Recent developments in electroceramics: MEMS applications for energy and environment, *Ceramic International, 30(7),* 2004, 1147-1154.

[2] C. Cui, R.H. Baughman, Z. lgbal, T.R. Kazmar, and D.K. Dalstrom, Improved piezoelectric ceramic/polymer composites for hydrophone applications, *Synthetic Metals, 85(1-3),* 1997, 1391-1392.

[3] C.J. Das, and D.K. Das-Gupta, Inorganic ceramic/polymer ferroelectric composite electrets, *IEEE Transactions on Dielectrics and Electrical Insulation, 3(5)*, 1996, 706-734.

[4] M. Arbatti, X. Shan, and Z-Y Cheng, Ceramic–polymer composites with high dielectric constant, *Advanced Materials*, *19*, 2007, 1369–1372.

[5] Z. Kutnjak, B. Vodopivec, D. Kuščer, M. Kosec, V. Bobnar, B. Hilczer, Calorimetric and dielectric study of vinylidene fluoride-trifluoroethylene-based composite, *Journal of Non-Crystalline Solids, 351(14-15)*, 2005, 1261-1265.

[6] S.H. Xie, B.K. Zhu, X.Z. Wei, Z.K. Xu, and Y.Y Xu, Polyimide/BaTiO$_3$ composites with controllable dielectric properties, *Composites Part A - Applied Science and Manufacturing, 36(8),* 2005, 1152-1157.

[7] T. Furukawa, K. Fujino, and E. Fukada, Electromechanical properties in the composites of epoxy resin and PZT ceramics, *Japanese Journal of Applied Physics, 15,* 1976, 2119–2129.

[8] W.W. Clegg, D.F.L. Jenkins, and M.J. Chunningham, The preparation of piezoceramic–polymer thick films and their application as micromechanical actuators. *Sensors and Actuators A, 58*, 1997, 173–177.

[9] W.K. Sakamoto, S. Shibatta-Kegesawa, D.H.F. Kanada, and D.K. Das-Gupta, Electrical properties of a composite of polyurethane and ferroelectric ceramics. *Journal of Materials Science, 33*, 1998, 3325–3329.

[10] H.C. Pant, M.K. Patra, A. Verma, S.R. Vadera, and N. Kumar, Study of the dielectric properties of Barium Titanate–polymer composites. *Acta Materialia, 54*, 2006, 3163–3169.

[11] L.A. Ramajo, M.M. Reboredo, and M.S. Castro, Characterisation of epoxy/BaTiO$_3$ composites processed by dipping for integral capacitor films (ICF). *Journal of Materials Science, 42*, 2007, 3685–3691.

[12] T. Takenaka., A. Huzumi, T. Hata, and K. Sakata, Mechanical properties of (Bi, Na)$_{1/2}$TiO$_3$-based piezoelectric ceramics. *Silicates Industrials 7(8),* 1993, 136-142.

[13] X.X. Wang, K.H. Lam, X.G. Tang, and H.L.W. Chan, Dielectric characteristics and polarization response of lead-free ferroelectric (Bi$_{0.5}$Na$_{0.5}$)$_{0.94}$Ba$_{0.06}$TiO$_3$-P(VDF-TrFE) 0-3 composites, *Solid State Communications, 130(10),* 2004, 695-699.

[14] K.H. Lam, X. Wang, and H.L.W. Chan, Piezoelectric and pyroelectric properties of Bi$_{0.5}$Na$_{0.5}$)$_{0.94}$Ba$_{0.06}$TiO$_3$/P(VDF-TrFE) 0-3 composites, *Composites. Part A – Applied Physics, 36(11)*, 2005, 1595-1599.

[15] A. K. Roy, A. Singh, K. Kumari, K. AmarNath, A. Prasad, and K. Prasad, Electrical properties and ac conductivity of (Bi$_{0.5}$Na$_{0.5}$)$_{0.94}$Ba$_{0.06}$TiO$_3$ ceramic, *ISRN Ceramics*, *vol. 2012,* 2012, Article ID 854831, 10 pages.

[16] R. Gerhardt, Impedance and dielectric spectroscopy revisited: distinguishing localized relaxation from long-range conductivity, *Journal of Physics and Chemistry of Solids, 55,* 1994, 1491–1506.

[17] V.M. Mohan, W. Qiu, J. Shen, and W. Chen, Electrical properties of poly(vinyl alcohol) (PVA) based on LiFePO$_4$ complex polymer electrolyte films, *Journal of Polymer Research 17,* 2010, 143–150.

[18] N.G. McCrum, B.E. Read, and G. Williams, *Anelastic and Dielectric Effects in Polymeric Solids* (Wiley & Sons, New York, 1967).

[19] D.C. Sinclair, and A.R. West, Impedance and modulus spectroscopy of semiconducting BaTiO$_3$ showing positive temperature coefficient of resistance, *Journal of Applied Physics, 66,* 1989, 3850-3856.

[20] D.C. Sinclair, and A.R. West, Effect of atmosphere on the PTCR properties of BaTiO$_3$ ceramics, *Journal of Materials Science, 29*, 1994, 6061-6068.

[21] K. Sambasiva Rao, K. Varada Rajuluuaa, B. Tilak, and A. Swathi, Effect of Ba^{2+} in BNT ceramics on dielectric and conductivity properties, *Natural Science 2 (4)*, 2010, 357-367.

[22] M.C. Steil, F. Thevenot, and M. Kleitz, Densification of yttria-stabilized zirconia: impedance spectroscopy analysis, *Journal of Electrochemical Society, 144,* 1997, 390-398

[23] E. Placzek-Popko, J. Trzmiel, Z. Gumienny, E. Wojtyna, and J. Szatkowski, Impedance spectroscopy of Au-CdTe:Ga Schottky contacts *Acta Physica Polonica A, 114(5)*, 2008, 1279-1283

[24] W.L. Warren, K. Vanheusden, D. Dimos, G. E. Pike, and B. A. Tuttle, Oxygen vacancy motion in perovskite oxides, *Journal of the American Ceramic Society*, *79(2)*, 1996, 536–538.

[25] F. A.Kröger, and H. J.Vink, Relations between the concentrations of imperfections in crystalline solids, *Solid State Physics, 3,* 1956, 307-435.

[26] M. J. Forbess, S. Seraji, Y. Wu, C. P. Nguyen, and G. Z. Cao, Dielectric properties of layered perovskite Sr$_{1-x}$A$_x$Bi$_2$Nb$_2$O$_9$ ferroelectrics (A=La, Ca and x = 0, 0.1), *Applied Physics Letters*, *76(20)*, 2000, 2934–2936.

[27] K. Funke, Jump relaxation in solid electrolytes, *Progress in Solid State Chemistry*, *22(2)*, 1993, 111–195.

[28] S. R. Elliot, AC conduction in amorphous chalcogenide and pnictide semiconductors, *Advances in Physics, 36,* 1987, 135–217.

[29] A. Pelaiz-Barranco, M. P. Gutierrez-Amador, A. Huanosta, and R. Valenzuela, Phase transitions in ferrimagnetic and ferroelectric ceramics by ac measurements, *Applied Physics Letters, 73(14)*, 1998, Article ID 2039, 3 pages,.

[30] S. Sumi, P. Prabhakar Rao, M. Deepa, and Koshy Peter, Electrical conductivity and impedance spectroscopy studies of cerium based aeschynite type semiconducting oxides CeTiMO$_6$ (M=Nb or Ta), *Journal of Applied Physics, 108*, 2010, 063718-063726.

[31] M.K. Fayek, S. Mostafa, F. Sayedahmed, S.S. Ata-Allah, and M. Kaiser, On the electrical behavior of nickel ferrite-gallates, *Journal of Magnetism and Magnetic Materials, 210*, 2000, 189-195.

[32] N. Ortega, A. Kumar, P. Bhattacharya, S.B. Majumdar, and R.S. Katiyar, Impedance spectroscopy of multiferroic PbZr$_x$Ti$_{1-x}$O$_3$/CoFe$_2$O$_4$ layered thin films, *Physical Review B, 77*, 2008, 014111-014120.

[33] D. Emin, Optical properties of large and small polarons and bipolarons, *Physical Review B, 48(18)*, 1993, 13691-13702.